Histol Histopathol (2022) 37: 335-348

**http://www.hh.um.es**

Histology and Histopathology
*From Cell Biology to Tissue Engineering*

**ORIGINAL ARTICLE** **Open Access**

# Circular RNA circFADS2 inhibits the progression of cutaneous squamous cell carcinoma by regulating miR-766-3p/HOXA9 axis

**Zhang Zhang[1], Huijun Sun[1], Junzhi Hou[2], Lili Li[3] and Lijuan Wu[4]**

[1]Department of Surgery, ShangQiu Medical College, Shangqiu City, [2]Department of Dermatology, ShangQiu City Hospital of Transitional Chinese Medicine, Shangqiu City, [3]Department of Obstetrics and Gynecology, Shangqiu Fifth People's Hospital, Shangqiu City and [4]Department of Surgery, Shangqiu Central Hospital, Shangqiu City, Henan Province, China

**Summary.** Background. Mounting evidence indicates that circular RNAs (circRNAs) play vital roles in human diseases, especially in cancers. However, the biological functions and underlying mechanism of circRNA fatty acid desaturase 2 (circFADS2) in cutaneous squamous cell carcinoma (CSCC) have not been reported.

Methods. The expression levels of circFADS2, microRNA-766-3p (miR-766-3p) and homeobox A9 (HOXA9) were determined by quantitative real-time PCR (qRT-PCR). Flow cytometry analysis was used to determine cell cycle distribution. Cell proliferation was evaluated by Cell Counting Kit-8 (CCK-8) and colony formation assays. Wound healing and transwell assays were used to assess cell migration and invasion abilities. Glycolysis was examined via the measurement of extracellular acidification rate (ECAR). All protein levels were detected by western blot assay. The interaction between miR-766-3p and circFADS2 or HOXA9 was predicted by bioinformatics software and confirmed by dual-luciferase reporter, RNA pull-down, and RNA Immunoprecipitation (RIP) assays. The mouse xenograft model was established to investigate the role of circFADS2 *in vivo*.

Results. CircFADS2 was downregulated in CSCC tissues and cells. CircFADS2 overexpression inhibited CSCC cell proliferation, metastasis and glycolysis. Moreover, miR-766-3p was able to directly bind to circFADS2, and circFADS2 played an anti-cancer role in CSCC by downregulating miR-766-3p. In addition, HOXA9 was a direct target of miR-766-3p, and miR-766-3p inhibition suppressed CSCC cell proliferation, metastasis and glycolysis by upregulating HOXA9. Furthermore, circFADS2 acted as a sponge of miR-766-3p to regulate HOXA9 expression. Besides, circFADS2 suppressed tumor growth in vivo.

Conclusion. CircFADS2 suppressed CSCC progression by regulating miR-766-3p/HOXA9 axis, which might provide a promising therapeutic target for CSCC.

**Key words:** Cutaneous squamous cell carcinoma, circFADS2, miR-766-3p, HOXA9

*Corresponding Author:* Zhang Zhang, MS, Department of Surgery, ShangQiu Medical College, No.666 Yingbin Road, Liangyuan District, Shangqiu 476000, Henan Province, China. e-mail: kcsb9x@126.com

DOI: 10.14670/HH-18-409

## Introduction

Cutaneous squamous cell carcinoma (CSCC) is the second most common skin cancer (Ratushny et al., 2012). Although outstanding advances have been made in therapeutic methods, the 5-year overall survival of CSCC patients is still unsatisfactory (25-50%) due to tumor aggressiveness and distant metastasis (Alam and Ratner, 2001; Keyal et al., 2019). Hence, it is imperative to screen effective therapeutic targets and determine the potential molecular mechanism of CSCC development.

Circular RNAs (circRNAs) are a type of non-coding RNAs (ncRNAs) with a circular covalent-closed structure which are generated from precursor mRNAs (pre-mRNAs) through back-splicing (Memczak et al., 2013). Many novel circRNAs have been identified in a variety of cancers (Wu et al., 2019). CircRNAs play crucial roles in regulating the progression of multiple diseases, including cancers (Haque and Harries, 2017; Meng et al., 2017). For example, circRNA_102171 was able to promote the progression of papillary thyroid cancer by regulating CTNNBIP1/β-catenin pathway (Bi et al., 2018). CircRNA cTFRC facilitated bladder cancer cell proliferation and metastasis (Su et al., 2019). CircRNA circSEPT9 mediated by E2F1 and EIF4A3 accelerated the carcinogenesis and development of breast cancer (Zheng et al., 2020). Moreover, several circRNAs have been demonstrated to play important roles in CSCC (Sand et al., 2016; Zhang et al., 2020).

However, more investigation about circRNA and CSCC is still further needed. As for circRNA fatty acid desaturase 2 (circFADS2; also known as hsa_circ_0022392), it is a novel circRNA, derived from the FADS2 gene, which is located at chr11:61630443-61631258. The data of GSE74758 (http://www.ncbi.nlm.nih.gov/geo/query/acc.cgi?acc=GSE74758) downloaded from the open Gene Expression Omnibus (GEO) database revealed that circFADS2 was significantly downregulated in CSCC tissues compared to normal skin tissues. So far, the biological roles and regulatory mechanism of circFADS2 in CSCC remain unclear.

The competing endogenous RNA (ceRNA) networks hypothesis shows that circRNAs can act as molecular sponges to interact with microRNAs (miRNAs) and then release genes that are targeted by specific miRNAs (Zhong et al., 2018; Bach et al., 2019). However, circRNA-miRNA-mRNA interactions in CSCC are still largely unknown and need further study. MiR-766-3p is a suspected inducer or inhibitor of tumor progression in different cancers (Li et al., 2015; Chen et al., 2017; You et al., 2018). Moreover, miR-766 has been reported to be upregulated CSCC tissues compared with normal cutaneous tissues and miR-766 functioned as a tumor promoter in CSCC (Liu et al., 2020a). Homeobox A9 (HOXA9), a member of the mammalian HOX family, has been reported be frequently dysregulated in many cancers and HOXA9 expression was downregulated in CSCC tissues relative to normal skin tissues (Zhou et al., 2018). However, to our knowledge, the relationship between circFADS2 and miR-766-3p and HOXA9 has not been explored. Intriguingly, bioinformatics tools showed that circFADS2 and HOXA9 shared the complementary binding sites for miR-766-3p. Therefore, we supposed that circFADS2/miR-766-3p/HOXA9 axis might be related to the progression of CSCC.

In our work, circFADS2 expression was investigated in CSCC tissues and cells. Additionally, we explored the ceRNA regulatory network of circFADS2/miR-766-3p/HOXA9 in CSCC, and also evaluated their effects on cell proliferation, metastasis and glycolysis. The purpose of this study was to establish a regulatory network to further understand CSCC pathogenesis. However, we did not pay attention to their roles in normal skin.

## Materials and methods

### *Specimen collection*

CSCC tissues (n=43) and adjacent normal tissues (ANT; n=43) were obtained from CSCC patients who underwent surgery at Pathology Laboratory, School of Basic Medicine, Shangqiu Medical College. Tissue specimens were harvested at surgery, promptly snap-frozen in liquid nitrogen and then preserved at -80°C. Informed consent was obtained from all patients. This study was approved by the Ethics Committee of Pathology Laboratory, School of Basic Medicine, Shangqiu Medical College.

### *Cell culture and transfection*

CSCC cell lines (SCL-1 and A-431) and human keratinocyte cell line (HaCaT) were purchased from BeNa Culture Collection (Beijing, China). The cell culture medium was Dulbecco's Modified Eagle's medium (Invitrogen, Carlsbad, CA, USA) including 10% fetal bovine serum (Invitrogen). All cells were maintained in a constant temperature incubator with 5% $CO_2$ at 37°C.

CircFADS2 overexpression plasmid (circFADS2) and matched control (vector), miR-766-3p mimics or inhibitor (miR-766-3p or anti-miR-766-3p) and matched control (miR-NC or anti-NC), small interfering RNAs (siRNAs) against HOXA9 (si-HOXA9#1, si-HOXA9#2, and si-HOXA9#3) and matched control (si-NC) were all obtained from RiboBio (Guangzhou, China). Lipofectamine 3000 (Invitrogen) was used for cell transfection.

### *Subcellular fractionation location*

Nuclear/Cytosol Fractionation Kit (Biovision, San Francisco Bay, CA, USA) was used to isolate the fractions of nuclear and cytosolic. In brief, A-431 cells were washed using the PBS and placed on ice. After that, these cells were suspended in fractionation buffer, followed by centrifugation (500×g; 5 min; 4°C). Next, the cytoplasmic fraction was acquired from the supernatant content, whereas the remaining nuclear pellet was again lysed using the cell disruption buffer as nuclear fraction. Finally, quantitative real-time polymerase PCR (qRT-PCR) was used to analyze the extracted RNAs from cytoplasmic and nuclear. Glyceraldehyde-3-phosphate dehydrogenase (GAPDH) functioned as a control for the cytoplasmic transcript, and U6 functioned as a control for the nuclear transcript.

### *RNase R and Actinomycin D treatment*

RNase R treatment was used to degrade linear RNA. Briefly, RNA (2 μg) was incubated with or without RNase R (3 U/μg; Epicentre Technologies, Madison, WI, USA) for 0.5 h at 37°C. Next, the treated RNAs were used for qRT-PCR to evaluate the abundance of circFADS2 and FADS2. For circFADS2 stability assay, Actinomycin D (2 mg/mL; Sigma-Aldrich, St. Louis, MO, USA) or dimethylsulphoxide (Sigma-Aldrich) was added into the cell culture medium. After treatment with Actinomycin D, the treated cells were collected and the corresponding levels were examined by qRT-PCR.

### *RNA isolation and qRT-PCR*

TRIzol reagent (Invitrogen) was used to isolate of total RNA. The cDNA was synthesized by PrimeScript RT Master Mix (for circRNA or mRNA; TaKaRa, Otsu, Japan) and miRNA reverse transcription PCR kit (for miRNA; RiboBio). Next, the cDNA was diluted and

subjected to qRT-PCR using SYBR Premix Ex Taq II (Takara) on CFX Real-time PCR system (Bio-Rad, Hercules, CA, USA). The RNA levels were evaluated with $2^{-\Delta\Delta Ct}$ method, followed by normalization to GAPDH (for circFADS2, FADS2 and HOXA9) and U6 (for miR-766-3p). Primer information was listed: circFADS2, (forward 5'-3': GGAGCAGTCCTTCT TCAACG; reverse 5'-3': GCCGTAGAAAGGGATG TAGG), FADS2 (forward 5'-3': TGCAACGTGGAGCA GTCCTTCT; reverse 5'-3': GGCACATAGAGACTTC ACCAGC), miR-766-3p (forward 5'-3': GCCGAGAC TCCAGCCCCACAG; reverse 5'-3': CAGTGCGTGTC GTGGAGT), HOXA9 (forward 5'-3': AGAATGAGAG CGGCGGAGACAA; reverse 5'-3': CTCTTTCTCC AGTTCCAGGGTC), GAPDH (forward 5'-3': TGGGGAAGGTGAAGGTCGG; reverse 5'-3': CTGGAAGATGGTGATGGGA), U6 (forward 5'-3': CTCGCTTCGGCAGCACATATACT; reverse 5'-3': CGCTTCACGAATTTGCGTGTCAT).

### *Flow cytometric analysis*

Cells were harvested after transfection for 48 h and then fixed in 70% ethanol (Beyotime, Jiangsu, China). After overnight fixation, the cells were treated with 25 μg/mL propidium iodide (PI; Sangon Biotech, Shanghai, China) and 100 μg/mL RNase A (Sangon Biotech). After incubation for 0.5 h at 37°C, flow cytometer (BD Biosciences, Franklin Lakes, NJ, USA) was applied to detect cell cycle distribution.

### *Cell counting kit-8 (CCK-8) assay*

CCK-8 assay was employed for measuring cell viability. Briefly, cells ($1\times10^3$ cells/well) were inoculated in a 96-well plate. After transfection, 10 μL CCK-8 (Beyotime) was placed into each well. Following incubation for 2-3 h at 37°C, 96-well plates were placed in a microplate reader (Bio-Rad) to determine the absorbance at 450 nm.

### *Colony formation assay*

Briefly, transfected cells were inoculated in a six-well plate and cultured for about 14 days to form colonies with the medium changed every 2-3 days. After incubation for14 days, 4% paraformaldehyde (1 mL/well; Beyotime) was added to per well to fix these colonies. After staining with 0.1% crystal violet (1 mL/well; Sigma-Aldrich) for 1-2 h, these colonies were counted by microscope (Olympus, Tokyo, Japan).

### *Wound healing assay*

Wound healing assay was utilized to detect migration ability of SCL-1 and A-431 cells. In short, SCL-1 and A-431 cells were inoculated in a 12-well plate. After transfection, confluent cells were scraped with a sterile pipette tip (200 μL) in the middle of each well. After washing with phosphate-buffered saline (PBS; Beyotime), the cells were cultured for 24 h. Images of these scratches were captured at 0 h and 24 h under a microscope (Olympus) with a magnification of ×40.

### *Transwell assay*

Transwell assay was performed by transwell inserts (Corning Costar, Corning, NY, USA) precoated with (for invasion assay) or without (for migration assay) Matrigel (BD Biosciences) in the upper chamber. SCL-1 and A-431 cells with serum-free media (0.2 mL) were inoculated in the upper chamber. Meanwhile, the complete medium (0.6 mL) was placed into the lower chamber. 24 h later, cells on the lower surface of the membrane were fixed with 4% paraformaldehyde (Beyotime) for 0.5 h, followed by staining with 0.1% crystal violet (Sigma-Aldrich) for 1 h. The stained cells were photographed under a microscope (Olympus) with a magnification of ×100.

### *Extracellular Acidification Rate (ECAR) measurement assay*

ECAR was tested using the Seahorse XF 96 Extracellular Flux Analyzer (Seahorse Bioscience, North Billerica, MA, USA). Briefly, cells (approximately $2\times10^4$) were placed in XF microplate, followed by baseline measurement. According to the specified time point, Glucose, oligomycin (OM) and 2glycolytic inhibitor (2-DG) were sequentially injected into each well. The data were determined using Seahorse XF 96 Wave software (Seahorse Bioscience).

### *Western blot assay*

Total protein was isolated using RIPA lysis buffer (Solarbio, Beijing, China). The protein was denatured by heating at 100°C for 3-5 min. After detection of protein concentration with bicinchoninic acid (BCA) protein assay kit (Abcam, Cambridge, UK), protein samples (about 30 μg/lane) were resolved and separated by 12% sodium dodecyl sulfate-polyacrylamide gel electrophoresis (SDS-PAGE; Solarbio), followed by transferring into nitrocellulose membranes (Invitrogen). After blocking with 5% non-fat milk, these membranes were incubated with primary antibodies for 12-14 h at 4°C. The primary antibodies, including cyclinD1 (ab226977, 1:2000), c-myc (ab39688; 1:500), matrix metalloproteinase 9 (MMP9) (ab38898; 1:1000), hexokinase 2 (HK2) (ab227198; 1:500), HOXA9 (ab191178; 1:1000), and β-actin (ab227387; 1:5000) were purchased from Abcam. Subsequently, these membranes were continuously probed with secondary antibody (ab205718/ab205719; 1:4000; Abcam). Finally, the enhanced chemiluminescence detection reagent (Solarbio) was utilized to visualize the protein bands.

### *Dual-luciferase reporter assay*

The candidate target miRNAs of circFADS2 were predicted using CircInteractome (https://circinteractome.nia.nih.gov/). The candidate target genes of miR-766-3p were predicted by TargetScan (http://www.targetscan.org/). The wild-type (WT) luciferase reporter vector of circFADS2 or HOXA9 (WT-circFADS2 or WT-3'UTR HOXA9) was synthesized by inserting the sequence of circFADS2 or HOXA9 containing the binding sites for miR-766-3p into pmirGLO luciferase reporter vector (Promega, Madison, WI, USA). At the same time, mutant (MUT) luciferase reporter vector of circFADS2 or HOXA9 (MUT-circFADS2 or MUT-3'UTR HOXA9) was generated by mutating the binding sites of miR-766-3p. After that, the constructed reporter plasmid and miR-766-3p or miR-NC were co-transfected into SCL-1 and A-431 cells. After being treated for 48 h, dual-Luciferase Reporter Assay System (Promega) was employed to measure the firefly and Renilla luciferase activities.

### *RNA pull-down assay*

Biotin labeled miR-NC (Bio-miR-NC) and miR-766-3p (Bio-miR-766-3p) were obtained from RiboBio, and were individually transfected into SCL-1 and A-431 cells. 48 h later, cell were collected and lysed using lysis buffer, followed by incubation with streptavidin beads (Invitrogen) at 4°C for 2 h. The RNA complexes combining on the beads were washed and used to detect the enrichment of circFADS2 by qRT-PCR.

### *RNA immunoprecipitation (RIP) assay*

RIP experiment was conducted using Magna RIP Kit (Millipore, Bedford, MA, USA). Briefly, cells at approximately 90% confluence were lysed by complete RIP lysis buffer. Afterward, RIP buffer including magnetic beads conjugated with anti-immunoglobulin G (anti-IgG) antibody (as negative control) or human anti-Argonaute2 (anti-Ago2) was added into cell lysates. Subsequently, the lysates were rotated overnight. Next, proteinase K was utilized to separate the RNA-protein complexes from beads. Finally, qRT-PCR was conducted to test the expression of circFADS2 and miR-766-3p.

### *In vivo assay*

For the in vivo tumor study, BALB/c nude mice (female; n=10; 6 weeks old; weighing 15-20 g) were provided by Vital River (Beijing, China). These mice were divided into 2 groups (n=5/group). A-431 cells ($1\times10^7$) stably transfected with circFADS2 and vector were subcutaneously injected into the right flank of each nude mouse. Tumor volume was calculated using the formula: Volume = 1/2 (length×width$^2$) and measured every three days. 27 days later, mice were sacrificed, and tumor tissues were excised and then the tissues were harvested for further study. Animal studies were approved by the Animal Care and Use Committee of Pathology Laboratory, School of Basic Medicine, Shangqiu Medical College.

### *Statistical analysis*

The data from at least three independent experiments were presented as the mean ± standard deviation (SD). Statistical analysis was performed by GraphPad Prism (GraphPad Software, San Diego California, USA). The Student's t-test was employed for analyzing differences between 2 groups, and one-way analysis of variance (ANOVA) was used when more than 2 groups were compared. Survival curve was generated by Kaplan-Meier method. Pearson's correlation coefficient was applied for detecting the correlation between miR-766-3p and circFADS2 or HOXA9. P value <0.05 was considered statistically significant. *P<0.05, **P<0.01, ***P<0.001.

## Results

### *The characteristics of circFADS2 in CSCC*

To identify the circRNAs involved in CSCC tumorigenesis, we first searched the GEO database. The data from the GEO database (accession number GSE74758) showed that circFADS2 was the most downregulated in CSCC tissues (Fig. 1A). CircFADS2 is generated from exons 8-10 of ASAP2 gene and is located on chromosome 11, whose spliced mature sequence length is 275 bp (Fig. 1B). Subsequently, the localization of circFADS2 was determined in A-431 cells. According to the qRT-PCR analysis, circFADS2 was mainly located in the cytoplasm (Fig. 1C). Next, we analyzed the characteristics of circFADS2 in CSCC cells. Results from qRT-PCR confirmed that circFADS2 was resistant to RNase R digestion (Fig. 1D), indicating the cyclic structure of circFADS2. Actinomycin D assay exhibited that the half-life of circFADS2 transcript exceeded 24 h, while the half-life of FADS2 mRNA was about 18 h (Fig. 1E). These results indicated that circFADS2 had a loop structure.

### *CircFADS2 was downregulated in CSCC*

To further confirm the expression of circFADS2 in CSCC tissues, qRT-PCR was performed. As displayed in Fig. 2A, circFADS2 expression was downregulated in CSCC tissues (n=43) relative to ANT (n=43). Additionally, the downregulated expression of circFADS2 was positively associated with lymphoid node metastasis (Fig. 2B). Moreover, 43 CSCC patients were divided into low circFADS2 (n=22) and high circFADS2 (n=21) expression groups according to median value of circFADS2 expression. Patients in low circFADS2 expression group showed poor survival compared with high expression group (p=0.0077) (Fig. 2C). Furthermore, circFADS2 expression was also

decreased in CSCC cells (SCL-1 and A-431) compared with that in HaCaT cells (Fig. 2D). These results indicated that circFADS2 might act as a tumor suppressor in CSCC.

### *CircFADS2 overexpression inhibited proliferation, metastasis and glycolysis in CSCC cells*

To investigate the potential biological functions of circFADS2 in CSCC, we overexpressed circFADS2 expression in SCL-1 and A-431 cells by transfection of circFADS2. As presented in Fig. 3A, transfection of circFADS2 obviously increased the expression of circFADS2, suggesting a high transfection efficiency. Cell cycle progression was analyzed using flow cytometry. Overexpression of circFADS2 increased the proportions of SCL-1 and A-431cells in G0/G1 phase, while it decreased the proportions of these cells in S phase, indicating that the cell cycle was arrested at the G0/G1 phase (Fig. 3B). CCK-8 and colony formation assays indicated that circFADS2 upregulation suppressed SCL-1 and A-431 cell viability and colony formation ability, indicating that circFADS2 was able to inhibit CSCC cell proliferation (Fig. 3C,D). Wound healing and transwell assays demonstrated that enforced expression of circFADS2 repressed SCL-1 and A-431 cell migration and invasion abilities (Fig. 3E,F). Glycolysis has been reported to promote the progression of CSCC (Zhou et al., 2018). Therefore, we investigated whether circFADS2 played an essential role in glycolysis in CSCC cells. The ECAR approximated the glycolysis flux rate, and we found that overexpression of circFADS2 decreased ECAR in SCL-1 and A-431 cells (Fig. 3G,H). CyclinD1, a member of a family of three closely associated D-type cyclins, is required for cell cycle progression in G1 and is a growth-promoting protein (Baldin et al., 1993). As one of the most essential transcriptional factors, c-myc expression is necessary for cancer cell proliferation (Gordan et al., 2007). MMP9 has been reported to play an important role in CSCC metastasis (Xia et al., 2013). Moreover, HK2 is a key rate-limiting enzyme in glucose metabolism and catalyzes the reaction of the first step of glycolysis, so HK2 plays a critical role in cancer glucose metabolism (Mathupala et al., 1997). Therefore, we explored the effect of circFADS2 on protein expression of cyclinD1, c-myc, MMP9, and HK2 in CSCC cells. We found that circFADS2 elevation led to the decrease in cyclinD1, c-myc, MMP9, and HK2 expression (Fig. 3I). All these findings suggested that circFADS2 limited cell cycle progression, proliferation, migration, invasion and glycolysis in CSCC cells.

### *CircFADS2 served as a sponge of miR-766-3p*

A previous study has reported that circRNAs can act as a molecular sponge to interact with miRNAs (Kulcheski et al., 2016). Next, we used an online

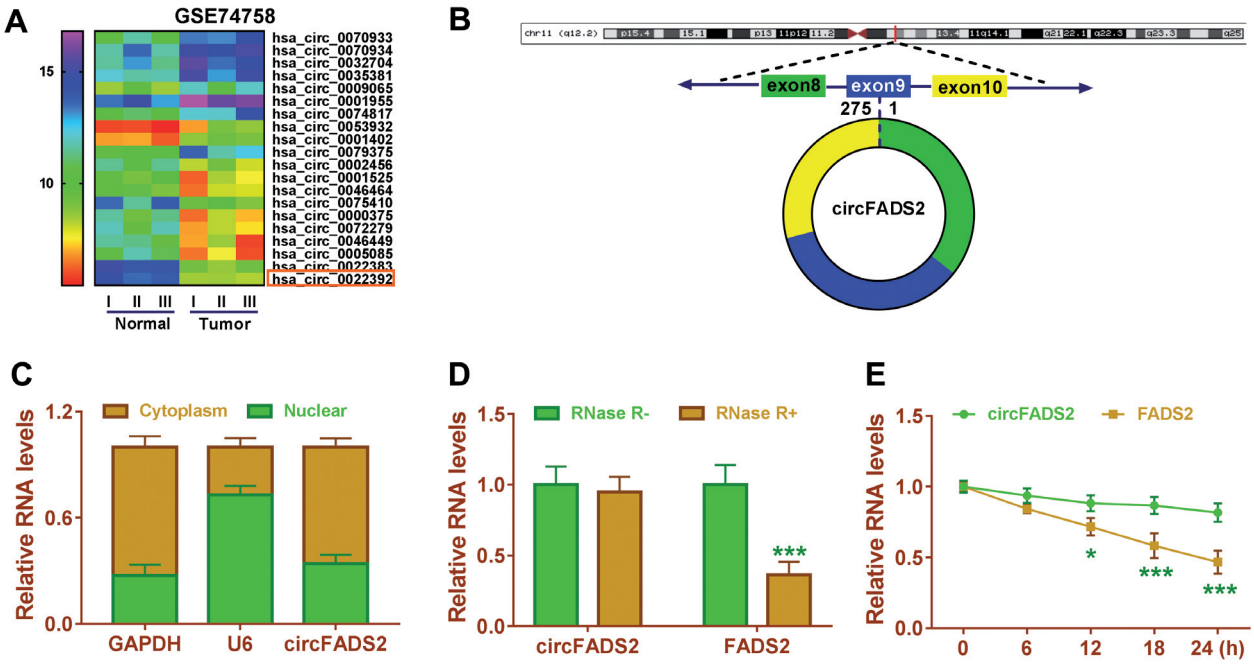


**Fig. 1.** Validation and characteristics of circFADS2. **A.** The heat map of GSE74758 showed the expression of 20 circRNAs in CSCC tissues and normal tissues. **B.** The basic formation of circFADS2 was presented. **C.** QRT-PCR was applied to determine the subcellular location of circFADS2 in A-431 cells. **D, E.** The levels of circFADS2 and FADS2 were determined after treatment of RNase R and Actinomycin D by qRT-PCR in A-431 cells. *P<0.05, **P<0.01, ***P<0.001.

bioinformatics database CircInteractome to predict the potential targets of circFADS2. As presented in Fig. 4A, 8 miRNAs had binding sites with circFADS2, and overexpression of circFADS2 reduced the expression of miR-1288 and miR-766-3p, and the expression of miR-766-3p decreased more. Therefore, we choose miR-766-3p for further study. The complementary binding sites of miR-766-3p and circFADS2 are shown in Fig. 4B. We found that the expression of miR-766-3p was increased by transfection of miR-766-3p and decreased by transfection of anti-miR-766-3p (Fig. 4C). To confirm the direct binding between miR-766-3p and circFADS2, dual-luciferase reporter, RNA pull-down and RIP assays were performed. As illustrated in Fig. 4D, introduction of miR-766-3p significantly inhibited the luciferase activity of WT-circFADS2, but had no obvious impact on the luciferase activity of MUT-circFADS2. RNA pull-down assay showed that the enrichment of circFADS2 was significantly increased in SCL-1 and A-431 cells transfection with Bio-miR-766-3p compared with the Bio-NC group (Fig. 4E). RIP assay indicated that the expression of circFADS2 and miR-766-3p was increased in Ago2-containing beads compared to the IgG control group (Fig. 4F). In addition, high expression of miR-766-3p was found in the CSCC group compared to the ANT group (Fig. 4G). An inverse correlation between circFADS2 and miR-766-3p expression was observed in CSCC tissues (Fig. 4H). As expected, miR-766-3p expression was increased in SCL-1 and A-431 cells in comparison with HaCaT cells (Fig. 4I). Moreover, we further confirmed that circFADS2 upregulation decreased the expression of miR-766-3p in SCL-1 and A-431 cells (Fig. 4J). Collectively, these data indicated that miR-766-3p was a direct target of circFADS2 in CSCC cells.

### *CircFADS2 regulated cell behavior by regulating miR-766-3p in CSCC cells*

Owing to the interaction between miR-766-3p and

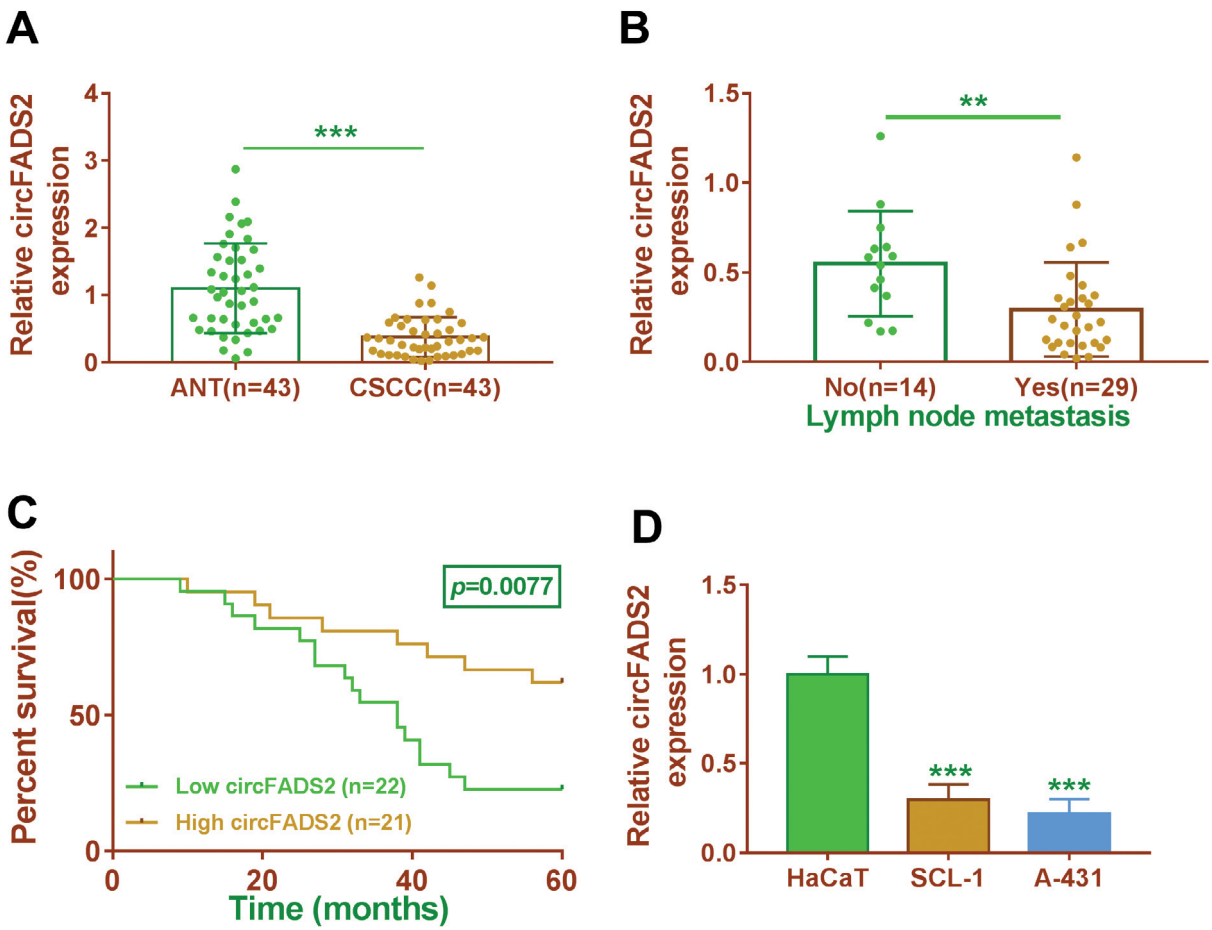


**Fig. 2.** The expression of circFADS2 was reduced in CSCC tissues and cells. **A.** The expression of circFADS2 was measured by qRT-PCR in CSCC tissues (n=43) and adjacent normal tissues (ANT; n=43). **B.** The expression of circFADS2 was determined uisng qRT-PCR in CSCC patients with or without lymphoid node metastasis. **C.** Kaplan-Meier method was performed to assess the effect of circFADS2 expression on survival rate in CSCC patients. **D.** The expression of circFADS2 was detected by qRT-PCR in CSCC cells (SCL-1 and A-431) and HaCaT cells. **P<0.01, ***P<0.001.

circFADS2, rescue assays were carried out to uncover the regulatory mechanism of circFADS2 in CSCC. Overexpression of miR-766-3p was able to reverse circFADS2 silence-mediated promotion of G0/G1 phase cells and reduction of S phase cells (Fig. 5A). Moreover, the inhibitory effects of circFADS2 overexpression on cell viability, colony formation ability, migration, invasion, and ECAR in CSCC cells were abolished by upregulating miR-766-3p (Fig. 5B-H). In addition, enforced expression of miR-766-3p was able to abate the reduction of cyclinD1, c-myc, MMP9, and HK2 expression induced by circFADS2 (Fig. 5I). Collectively, these results demonstrated that circFADS2 exerted its effects by targeting miR-766-3p in CSCC cells.

### *HOXA9 was a direct target of miR-766-3p*

To further explore the underlying mechanism by which miR-766-3p exerted its roles in CSCC cells, TargetScan was used and identified HOXA9 as a potential downstream target of miR-766-3p (Fig. 6A). The dual-luciferase reporter assay showed that miR-766-3p upregulation significantly reduced the luciferase activity of WT-3'UTR HOXA9, but not MUT-3'UTR HOXA9 in SCL-1 and A-431 cells (Fig. 6B). Next, we explored HOXA9 expression in CSCC tissues. Results showed that HOXA9 mRNA expression was decreased in CSCC tissues compared to ANT (Fig. 6C). In addition, correlation analysis showed that HOXA9 mRNA expression was inversely correlated with miR-766-3p expression in CSCC tissues (Fig. 6D). Moreover, HOXA9 protein expression was also reduced in CSCC tissues and cells (SCL-1 and A-431) relative to ANT and HaCaT cells (Fig. 6E,F). In addition, we found that miR-766-3p overexpression reduced the protein expression of HOXA9, whereas miR-766-3p inhibition promoted the protein expression of HOXA9 (Fig. 6G). To determine whether circFADS2 and miR-766-3p regulated the expression of HOXA9, we transfected SCL-1 and A-431 cells with vector, circFADS2, circFADS2 + miR-NC, or circFADS2 + miR-766-3p. As detected by western blot, overexpression of circFADS2 promoted the protein expression of HOXA9, which was attenuated by upregulating miR-766-3p (Fig. 6H), suggesting that circFADS2 promoted HOXA9 expression by sponging miR-766-3p.

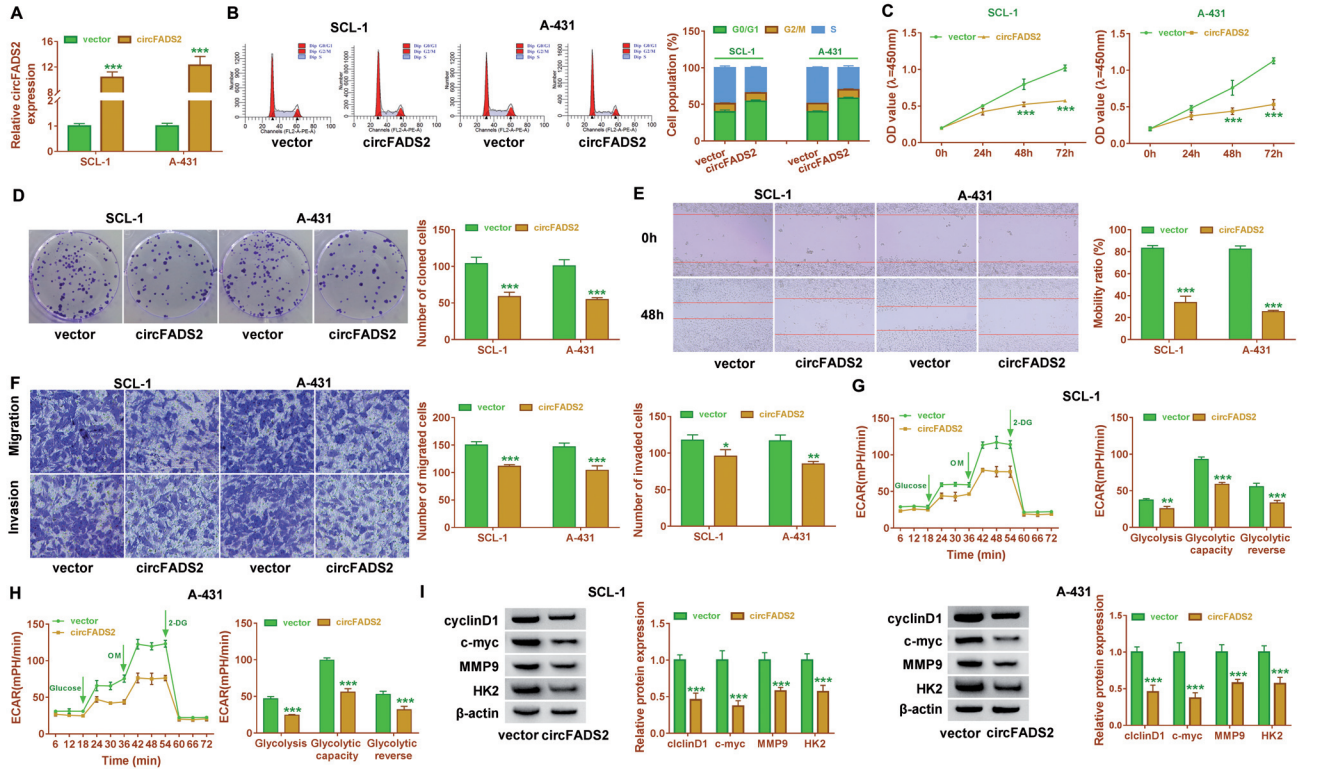


**Fig. 3.** Upregulaiton of circFADS2 suppressed CSCC cell proliferation, metastasis and glycolysis. SCL-1 and A-431 cells were transfected with vector or circFADS2. **A.** The expression of circFADS2 was determined by qRT-PCR. **B.** Flow cytometry analysis was employed to determine cell cycle distribution. **C.** CCK-8 assay was used to assess cell viability. **D.** Colony formation assay was utilized to measure colony formation ability. **E.** Wound healing assay was employed to assess cell migration ability (×40). **F.** Transwell assay was utilized to evaluate cell migration and invasion abilities (×100). **G, H.** ECAR was detected using a Seahorse XF 96 Extracellular Flux Analyzer. **I.** The protein levels of cyclinD1, c-myc, MMP9, and HK2 were determined by western blot. *P<0.05, **P<0.01, ***P<0.001.

### *MiR-766-3p inhibition suppressed CSCC cell proliferation, metastasis and glycolysis by targeting HOXA9*

Next, rescue experiments were performed to determine whether miR-766-3p exerted its roles in CSCC cells by targeting HOXA9. Western blot assay indicated that transfection of si-HOXA9#1, si-HOXA9#2, or si-HOXA9#3 reduced the protein expression of HOXA9, and transfection of si-HOXA9#3 reduced the most (Fig. 7A). Thus, si-HOXA9#3 was selected for further research. Transfection of anti-miR-766-3p promoted the protein expression of HOXA9, which was restored by co-transfection of si-HOXA9#3 (Fig. 7B). Inhibition of miR-766-3p arrested SCL-1 and A-431 cells in the G0/G1 phase, which was reversed by downregulating HOXA9 (Fig. 7C). Moreover, downregulation of miR-766-3p decreased cell viability and the number of cloned cells in SCL-1 and A-431 cells, and knockdown of HOXA9 mitigated the effect of anti-miR-766-3p (Fig. 7D,E). Similarly, miR-766-3p downregulation in SCL-1 and A-431 cells resulted in inhibition of migration and invasion, which could be abrogated by HOXA9 silence (Fig. 7F-H). Furthermore,

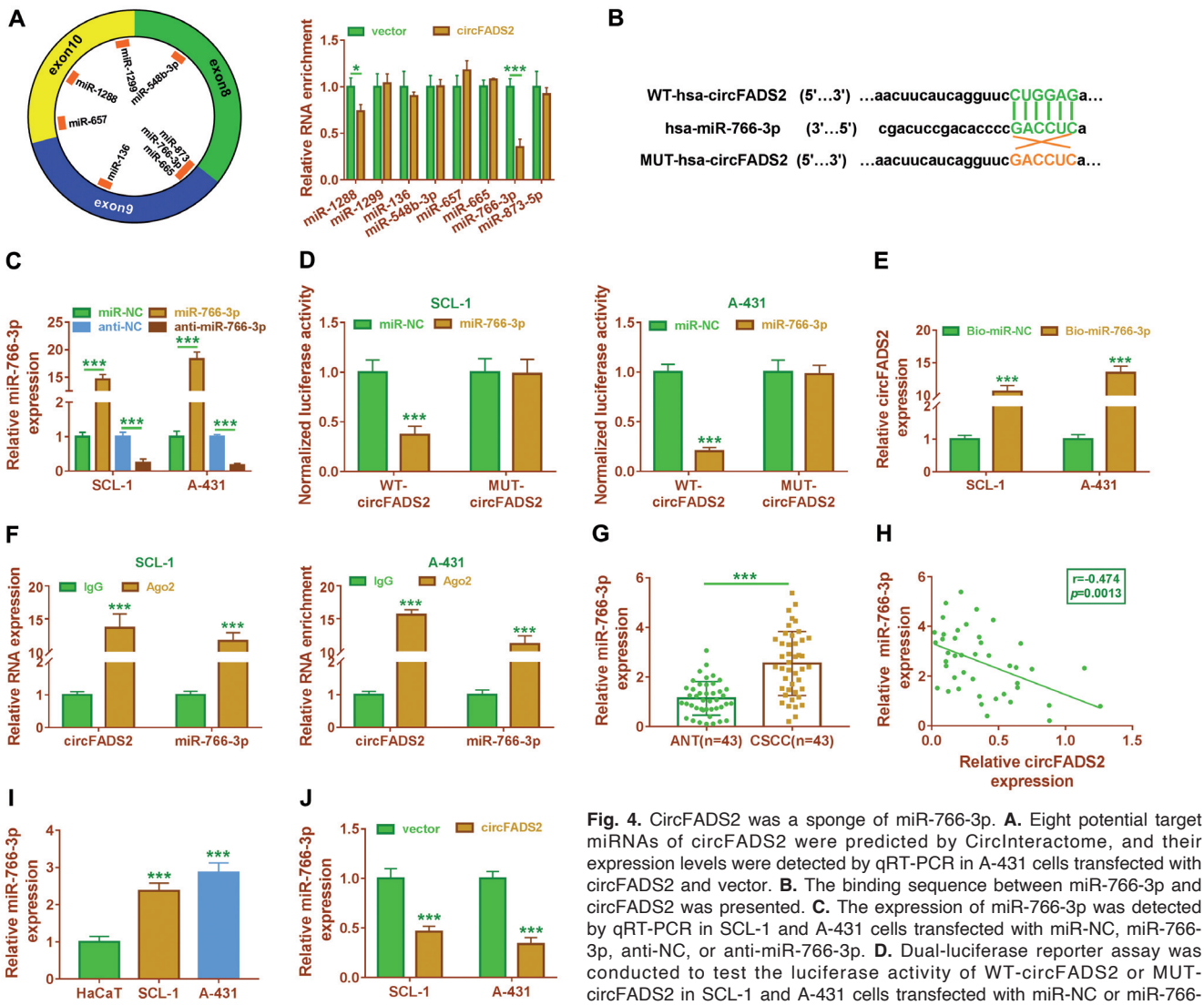


**Fig. 4.** CircFADS2 was a sponge of miR-766-3p. **A.** Eight potential target miRNAs of circFADS2 were predicted by CircInteractome, and their expression levels were detected by qRT-PCR in A-431 cells transfected with circFADS2 and vector. **B.** The binding sequence between miR-766-3p and circFADS2 was presented. **C.** The expression of miR-766-3p was detected by qRT-PCR in SCL-1 and A-431 cells transfected with miR-NC, miR-766-3p, anti-NC, or anti-miR-766-3p. **D.** Dual-luciferase reporter assay was conducted to test the luciferase activity of WT-circFADS2 or MUT-circFADS2 in SCL-1 and A-431 cells transfected with miR-NC or miR-766-3p. **E.** The expression of circFADS2 was detected by RNA pull-down assay and qRT-PCR in SCL-1 and A-431 cells transfected with Bio-miR-NC or Bio-miR-766-3p. **F.** The expression of circFADS2 and miR-766-3p was determined by RIP assay and qRT-PCR in SCL-1 and A-431 cells. **G.** The expression of miR-766-3p was examined by qRT-PCR in CSCC tissues and ANT. **H.** Correlation between the expression of circFADS2 and miR-766-3p was assessed in CSCC tissues by Pearson's correlation test. **I.** The expression of miR-766-3p was detected by qRT-PCR in HaCaT, SCL-1 and A-431 cells. **J.** The expression of miR-766-3p was measured using qRT-PCR in SCL-1 and A-431 cells transfected with vector and circFADS2. *P<0.05, ***P<0.001.

miR-766-3p downregulation reduced ECAR in SCL-1 and A-431 cells, while HOXA9 knockdown was able to counteract this inhibitory effect (Fig. 7I,J). Meanwhile, the protein levels of cyclinD1, c-myc, MMP9, and HK2 were reduced by inhibiting miR-766-3p, which was abolished by silencing HOXA9 (Fig. 7K). These results indicated that miR-766-3p exerted its roles by targeting HOXA9 in CSCC cells.

### *CircFADS2 overexpression reduced tumor growth in vivo*

To confirm the anti-tumor role of circFADS2 in vivo, we established a mouse xenograft model of CSCC by subcutaneous inoculation of A-431 cells stably transfected with circFADS2 or vector. We found that tumor volume and weight were inhibited in circFADS2 group (Fig. 8A,B). Subsequently, qRT-PCR showed that circFADS2 overexpression increased the expression of circFADS2 and decreased the expression of miR-766-3p in tumor tissues (Fig. 8C). Besides, western blot assay demonstrated that HOXA9 was upregulated and cyclinD1, c-myc, MMP9, and HK2 were downregulated in circFADS2-derived tumor tissues (Fig. 8D). The above results indicated that circFADS2 overexpression suppressed CSCC tumorigenesis through miR-766-3p/HOXA9 axis.

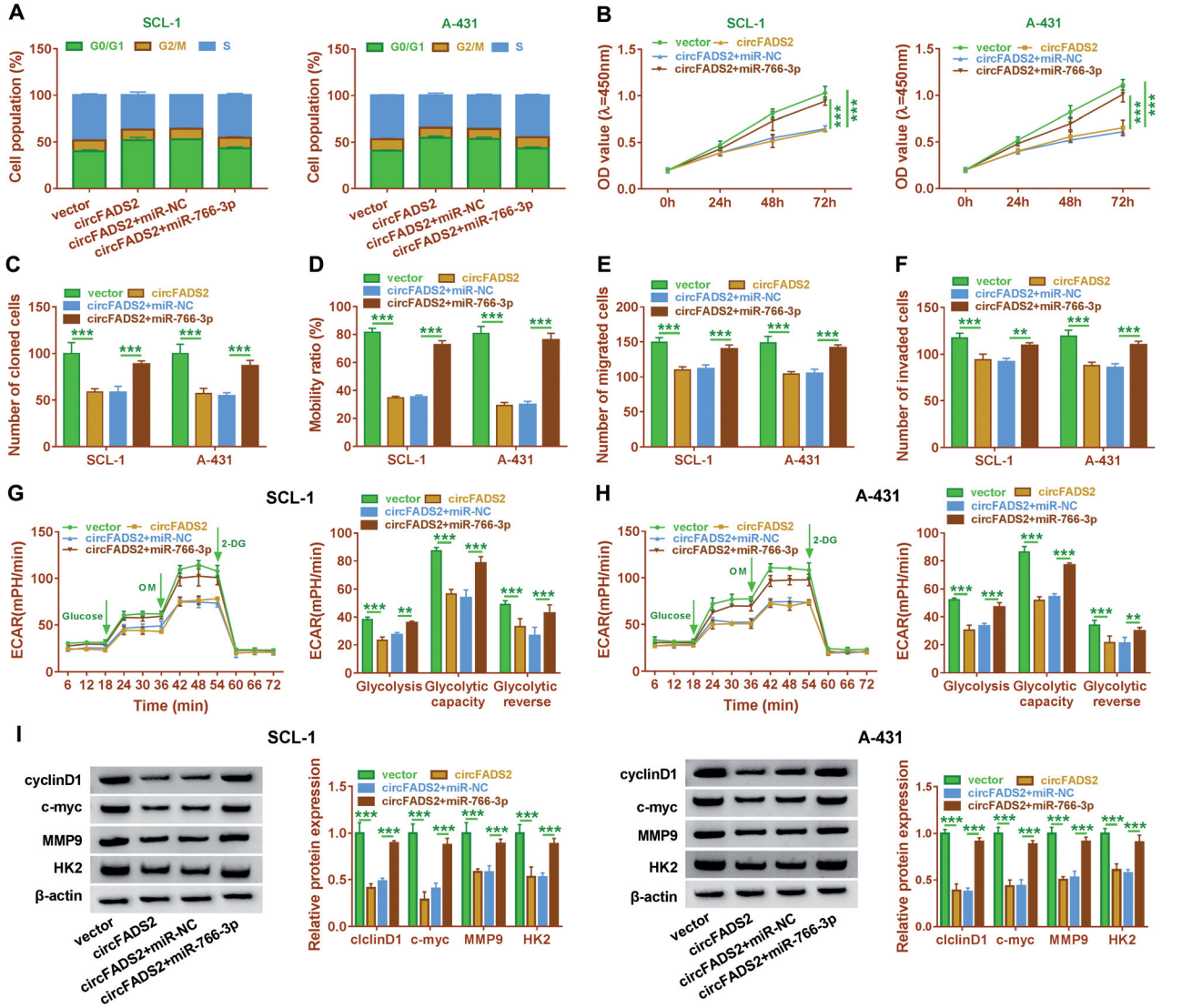


**Fig. 5.** CircFADS2 affected CSCC cell proliferation, metastasis and glycolysis by regulating miR-766-3p. SCL-1 and A-431 cells were transfected with vector, circFADS2, circFADS2 + miR-NC, or circFADS2 + miR-766-3p. **A.** Cell cycle distribution was determined by flow cytometry analysis. **B, C.** Cell proliferation was determined by CCK-8 assay and colony formation assay. **D-F.** Wound healing assay and transwell assay were conducted to evaluate cell migration and invasion abilities. **G, H.** ECAR was detected using a Seahorse XF 96 Extracellular Flux Analyzer. **I.** Western blot assay was carried out to examine the protein expression of cyclinD1, c-myc, MMP9, and HK2. **P<0.01, ***P<0.001.

## Discussion

Due to the high degree of invasiveness, the recurrence and mortality of CSCC patients are still high (Samarasinghe et al., 2011). In our research, we aimed to find a novel regulatory mechanism in the occurrence and development of CSCC. Recently, aberrant expression of circRNA has been suggested to be closely associated with the progression of multiple cancers, including CSCC (Wang et al., 2017b). Here, we demonstrated that circFADS2 inhibited CSCC progression by serving as a miR-766-3p sponge to mediate HOXA9 expression.

CircFADS2 has been demonstrated to play essential roles in some cancers. For instance, circFADS2 was increased in lung cancer tissues, and circFADS2 inhibition inhibited lung cancer cell proliferation and invasion ability by sponging miR-498 (Zhao et al., 2018). Moreover, the expression of circFADS2 was increased in colorectal cancer tissues and higher expression of circFADS2 had shorter overall survival time (Xiao et al., 2020). Differently, we revealed that circFADS2 expression was downregulated in CSCC tissues and cells, and lower expression of circFADS2 had shorter overall survival time, indicating that circFADS2 might serve as a promising prognostic biomarker for CSCC. Several studies revealed that circRNAs were involved in regulating CSCC cellular processes, such as proliferation, invasion and apoptosis

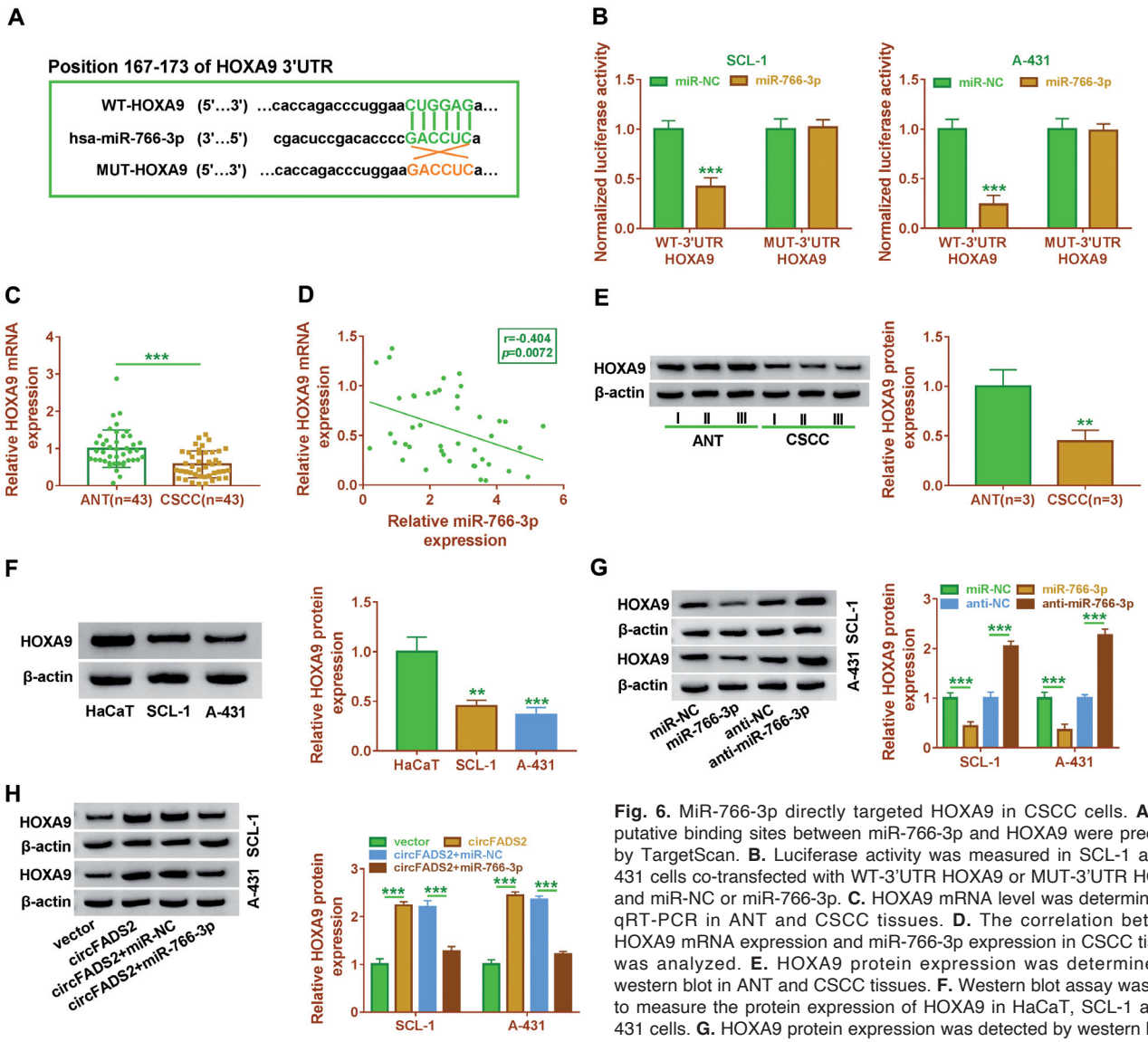


**Fig. 6.** MiR-766-3p directly targeted HOXA9 in CSCC cells. **A.** The putative binding sites between miR-766-3p and HOXA9 were predicted by TargetScan. **B.** Luciferase activity was measured in SCL-1 and A-431 cells co-transfected with WT-3'UTR HOXA9 or MUT-3'UTR HOXA9 and miR-NC or miR-766-3p. **C.** HOXA9 mRNA level was determined by qRT-PCR in ANT and CSCC tissues. **D.** The correlation between HOXA9 mRNA expression and miR-766-3p expression in CSCC tissues was analyzed. **E.** HOXA9 protein expression was determined by western blot in ANT and CSCC tissues. **F.** Western blot assay was used to measure the protein expression of HOXA9 in HaCaT, SCL-1 and A-431 cells. **G.** HOXA9 protein expression was detected by western blot in SCL-1 and A-431 cells transfected with miR-NC, miR-766-3p, anti-NC, or anti-miR-766-3p. **H.** The protein expression of HOXA9 was examined by western blot in SCL-1 and A-431 cells transfected with vector, circFADS2, circFADS2 + miR-NC, or circFADS2 + miR-766-3p. **P<0.01, ***P<0.001.

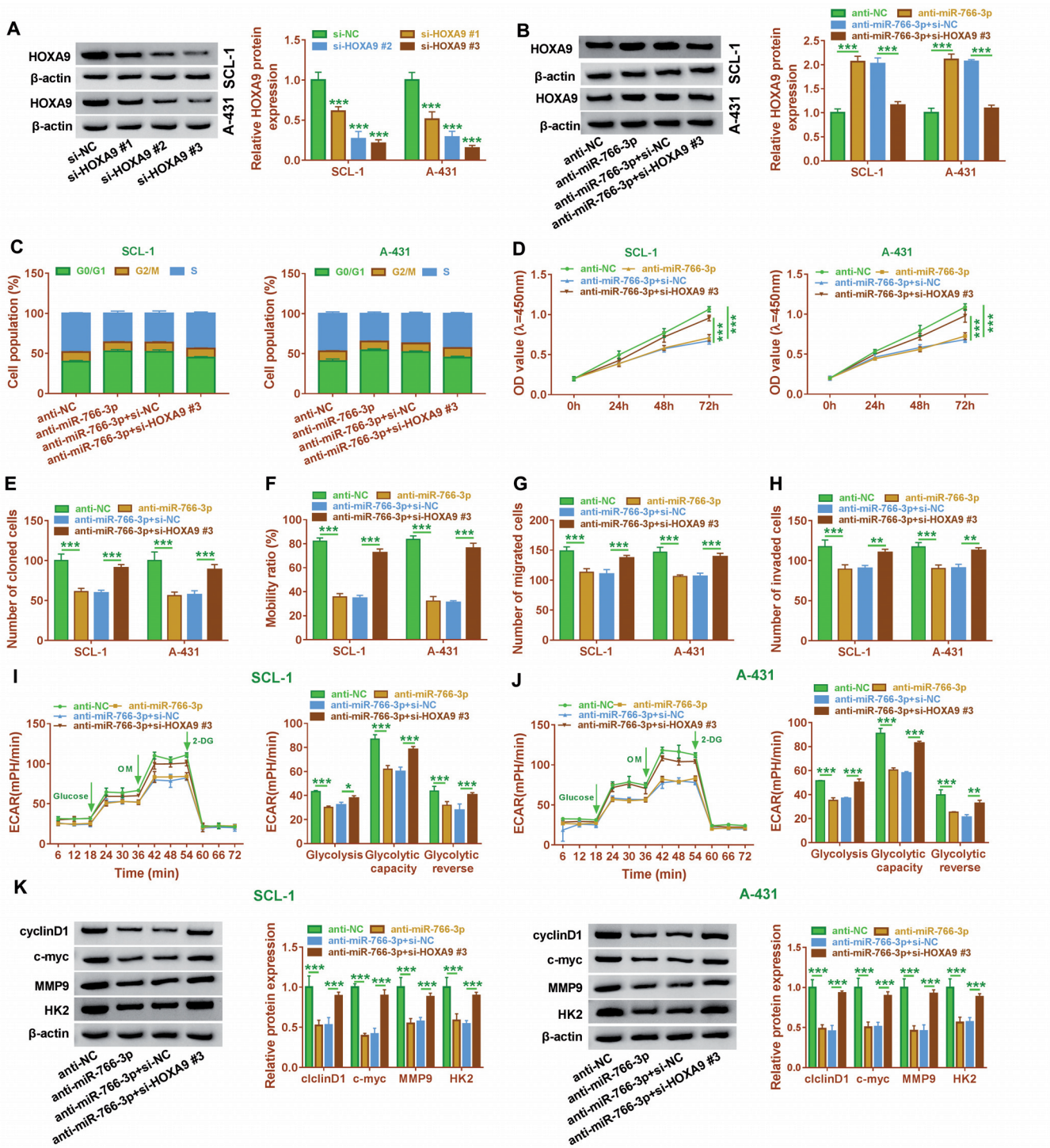


**Fig. 7.** MiR-766-3p regulated CSCC cell proliferation, metastasis and glycolysis by targeting HOXA9. **A.** HOXA9 protein expression was determined by western blot in SCL-1 and A-431 cells transfected with si-NC, si-HOXA9#1, si-HOXA9#2, or si-HOXA9#3. (B-K) SCL-1 and A-431 cells were transfected with anti-NC, anti-miR-766-3p, anti-miR-766-3p + si-NC, or anti-miR-766-3p + si-HOXA9#3. **B.** HOXA9 protein expression was measured by western blot assay. **C.** Flow cytometry analysis was used for measuring cell cycle distribution. **D, E.** Colony formation and CCK-8 assays were employed to determine cell proliferation ability. **F-H.** Wound healing assay and transwell assay were employed to assess cell migration and invasion capacities. **I, J.** ECAR was examined by Seahorse XF 96 Extracellular Flux Analyzer. **K.** Western blot assay was conducted to determine the protein levels of cyclinD1, c-myc, MMP9, and HK2. *P<0.05, **P<0.01, ***P<0.001.

(An et al., 2019; Gao et al., 2020). Nevertheless, the association between circRNAs and CSCC progression remains poorly understood, and the biological function of circFADS2 in CSCC is still unclear. Herein, we observed that circFADS2 upregulation inhibited CSCC cell proliferation, metastasis and glycolysis, and also suppressed tumor growth of CSCC in vivo, suggesting that circFADS2 acted as a tumor-suppressing circRNA in CSCC.

The most well-established theory is that circRNAs located in the cytoplasm can serve as miRNA sponges to upregulate the expression of target mRNAs (Hansen et al., 2013). In this research, we demonstrated that circFADS2 was primarily located in the cytoplasm. Therefore, we hypothesized that circFADS2 might regulate CSCC progression by directly binding to miRNAs. Then, the target miRNAs for circFADS2 were predicted by bioinformatics analysis (CircInteractome), and we observed that circFADS2 might bind to miR-766-3p, which was verified by a series of experiments. MiR-766-3p has been shown to act as an important regulator in some cancers. For instance, You et al. declared that miR-766-3p inhibited hepatocellular carcinoma progression by targeting Wnt3a (You et al., 2018). By contrast, Zhang et al. disclosed that miR-766-3p accelerated esophageal squamous cell carcinoma cell migration and invasion (Liu et al., 2020b). A microarray analysis by Sand et al. has demonstrated that miR-766 was overexpressed in CSCC tissue samples (Sand et al., 2012). More importantly, Liu et al. demonstrated that miR-766 was upregulated in CSCC tissue samples and cell lines, and miR-766 contributed to CSCC cell proliferation, migration and invasion by targeting PDCD5 (Liu et al., 2020a). Consistently, we uncovered that miR-766-3p was also upregulated in CSCC tissue specimens and cell lines. Rescue experiments proved that miR-766-3p abated the suppressive influence of circFADS2 on cell proliferation, metastasis and glycolysis in CSCC cells. These findings strongly suggest that circFADS2 can exert its biological functions in CSCC cells by sponging miR-766-3p.

MiRNAs are known to exert their roles by directly binding to target mRNAs (Felekkis et al., 2010). Therefore, the potential targets of miR-766-3p were predicted by bioinformatics tool (TargetScan). We confirmed that miR-766-3p directly interacted with HOXA9. Up to now, the functions of HOXA9 in cancers have been controversial. HOXA9 acts as a tumor suppressor in some malignancies, including cervical cancer (Alvarado-Ruiz et al., 2016), breast cancer (Gilbert et al., 2010), and lung cancer (Hwang et al., 2015), or as a tumor facilitator in others, such as ovarian cancer (Ko et al., 2012), colorectal cancer (Wang et al., 2017b), and gastric cancer (Ma et al., 2017). HOXA9 was reported to be lowly expressed in CSCC and it plays an anti-tumor role in CSCC via inhibiting glycolysis,

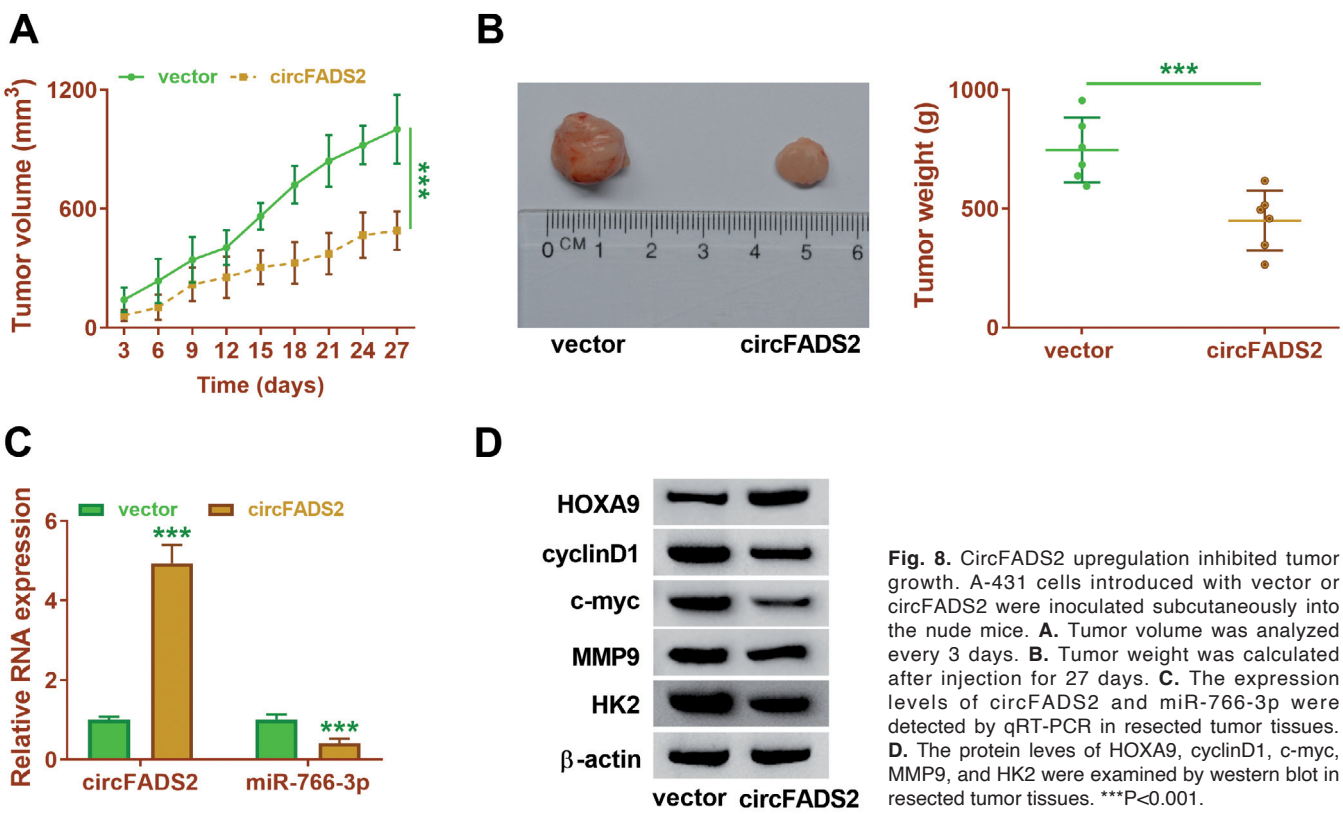


**Fig. 8.** CircFADS2 upregulation inhibited tumor growth. A-431 cells introduced with vector or circFADS2 were inoculated subcutaneously into the nude mice. **A.** Tumor volume was analyzed every 3 days. **B.** Tumor weight was calculated after injection for 27 days. **C.** The expression levels of circFADS2 and miR-766-3p were detected by qRT-PCR in resected tumor tissues. **D.** The protein leves of HOXA9, cyclinD1, c-myc, MMP9, and HK2 were examined by western blot in resected tumor tissues. ***P<0.001.

proliferation and migration and promoting apoptosis (Zhou et al., 2018; Han et al., 2019). Consistent with previous research, we revealed that HOXA9 expression was reduced in CSCC tissues and cells. Additionally, silence of HOXA9 abated the suppressive impact of anti-miR-766-3p on CSCC cell proliferation, metastasis and glycolysis. Moreover, circFADS2 positively regulated HOXA9 expression through sponging miR-766-3p in CSCC cells. Collectively, these data revealed that circFADS2 affected cell growth, metastasis, glycolysis, and tumor growth by regulating miR-766-3p and HOXA9 in CSCC.

In conclusion, circFADS2 expression was downregulated in CSCC tissues and cells. Overexpression of circFADS2 repressed CSCC progression by inhibiting miR-766-3p and promoting HOXA9 expression. Our study is the first to elucidate the circFADS2/miR-766-3p/HOXA9 regulatory network in CSCC cells. The study might offer a promising therapeutic target for treatment of CSCC or other diseases.

*Acknowledgements.* None

*Disclosure of interest.* The authors declare that they have no financial conflict of interest.

*Funding.* None.

*Ethics approval and consent participate.* Written informed consent was obtained from patients with approval by the Institutional Review Board in Pathology Laboratory, School of Basic Medicine, Shangqiu Medical College.

*Data availability.* Please contact the correspondence author for the data request.

*Authors' contribution.* Zhang Zhang was responsible for drafting the manuscript. Huijun Sun and Junzhi Hou contributed to the analysis and interpretation of data. Lili Li and Lijuan Wu contributed in the data collection. All authors read and approved the final manuscript.

## References

Alam M. and Ratner D. (2001). Cutaneous squamous-cell carcinoma. N. Engl. J. Med. 344, 975-983.

Alvarado-Ruiz L., Martinez-Silva M.G., Torres-Reyes L.A., Pina-Sanchez P., Ortiz-Lazareno P., Bravo-Cuellar A., Aguilar-Lemarroy A. and Jave-Suarez L.F. (2016). Hoxa9 is underexpressed in cervical cancer cells and its restoration decreases proliferation, migration and expression of epithelial-to-mesenchymal transition genes. Asian Pac. J. Cancer Prev. 17, 1037-1047.

An X., Liu X., Ma G. and Li C. (2019). Upregulated circular RNA circ_0070934 facilitates cutaneous squamous cell carcinoma cell growth and invasion by sponging miR-1238 and miR-1247-5p. Biochem. Biophys. Res. Commun. 513, 380-385.

Bach D.H., Lee S.K. and Sood A.K. (2019). Circular RNAs in cancer. Mol. Ther. Nucleic Acids 16, 118-129.

Baldin V., Lukas J., Marcote M.J., Pagano M. and Draetta G. (1993). Cyclin D1 is a nuclear protein required for cell cycle progression in G1. Genes Dev. 7, 812-821.

Bi W., Huang J., Nie C., Liu B., He G., Han J., Pang R., Ding Z., Xu J. and Zhang J. (2018). CircRNA circRNA_102171 promotes papillary thyroid cancer progression through modulating CTNNBIP1-dependent activation of β-catenin pathway. J. Exp. Clin. Cancer Res. 37, 275.

Chen C., Xue S., Zhang J., Chen W., Gong D., Zheng J., Ma J., Xue W., Chen Y., Zhai W. and Zheng J. (2017). DNA-methylation-mediated repression of miR-766-3p promotes cell proliferation via targeting SF2 expression in renal cell carcinoma. Int. J. Cancer 141, 1867-1878.

Felekkis K., Touvana E., Stefanou C. and Deltas C. (2010). MicroRNAs: A newly described class of encoded molecules that play a role in health and disease. Hippokratia 14, 236.

Gao L., Jin H.J., Zhang D. and Lin Q. (2020). Silencing circRNA_001937 may inhibit cutaneous squamous cell carcinoma proliferation and induce apoptosis by preventing the sponging of the miRNA-597-3p/FOSL2 pathway. Int. J. Mol. Med. 46, 1653-1660.

Gilbert P.M., Mouw J.K., Unger M.A., Lakins J.N., Gbegnon M.K., Clemmer V.B., Benezra M., Licht J.D., Boudreau N.J., Tsai K.K., Welm A.L., Feldman M.D., Weber B.L. and Weaver V.M. (2010). HOXA9 regulates BRCA1 expression to modulate human breast tumor phenotype. J. Clin. Invest. 120, 1535-1550.

Gordan J.D., Thompson C.B. and Simon M.C. (2007). HIF and c-Myc: Sibling rivals for control of cancer cell metabolism and proliferation. Cancer Cell 12, 108-113.

Han S., Li X., Liang X. and Zhou L. (2019). HOXA9 transcriptionally promotes apoptosis and represses autophagy by targeting NF-κB in cutaneous squamous cell carcinoma. Cells 8, 1360.

Hansen T.B., Jensen T.I., Clausen B.H., Bramsen J.B., Finsen B., Damgaard C.K. and Kjems J. (2013). Natural RNA circles function as efficient microRNA sponges. Nature 495, 384-388.

Haque S. and Harries L.W. (2017). Circular RNAs (circRNAs) in health and disease. Genes 8, 353.

Hwang J.A., Lee B.B., Kim Y., Hong S.H., Kim Y.H., Han J., Shim Y.M., Yoon C.Y., Lee Y.S. and Kim D.H. (2015). HOXA9 inhibits migration of lung cancer cells and its hypermethylation is associated with recurrence in non-small cell lung cancer. Mol. Carcinog. 54 (Suppl. 1), E72-80.

Keyal U., Bhatta A.K., Zhang G. and Wang X.L. (2019). Present and future perspectives of photodynamic therapy for cutaneous squamous cell carcinoma. J. Am. Acad. Dermatol. 80, 765-773.

Ko S.Y., Barengo N., Ladanyi A., Lee J.S., Marini F., Lengyel E. and Naora H. (2012). HOXA9 promotes ovarian cancer growth by stimulating cancer-associated fibroblasts. J. Clin. Invest. 122, 3603-3617.

Kulcheski F.R., Christoff A.P. and Margis R. (2016). Circular RNAs are miRNA sponges and can be used as a new class of biomarker. J. Biotechnol. 238, 42-51.

Li Y.C., Li C.F., Chen L.B., Li D.D., Yang L., Jin J.P. and Zhang B. (2015). MicroRNA-766 targeting regulation of SOX6 expression promoted cell proliferation of human colorectal cancer. Onco Targets Ther. 8, 2981-2988.

Liu P., Shi L., Ding Y., Luan J., Shan X., Li Q. and Zhang S. (2020a). MicroRNA-766 promotes the proliferation, migration and invasion, and inhibits the apoptosis of cutaneous squamous cell carcinoma cells by targeting PDCD5. Onco. Targets Ther. 13, 4099-4110.

Liu S., Lin Z., Zheng Z., Rao W., Lin Y., Chen H., Xie Q., Chen Y. and Hu Z. (2020b). Serum exosomal microRNA-766-3p expression is associated with poor prognosis of esophageal squamous cell carcinoma. Cancer Sci. 111, 3881-3892.

Ma Y.Y., Zhang Y., Mou X.Z., Liu Z.C., Ru G.Q. and Li E. (2017). High

level of homeobox A9 and PBX homeobox 3 expression in gastric cancer correlates with poor prognosis. Oncol. Lett. 14, 5883-5889.

Mathupala S.P., Rempel A. and Pedersen P.L. (1997). Aberrant glycolytic metabolism of cancer cells: A remarkable coordination of genetic, transcriptional, post-translational, and mutational events that lead to a critical role for type II hexokinase. J. Bioenerg. Biomembr. 29, 339-343.

Memczak S., Jens M., Elefsinioti A., Torti F., Krueger J., Rybak A., Maier L., Mackowiak S.D., Gregersen L.H., Munschauer M., Loewer A., Ziebold U., Landthaler M., Kocks C., le Noble F. and Rajewsky N. (2013). Circular RNAs are a large class of animal RNAs with regulatory potency. Nature 495, 333-338.

Meng S., Zhou H., Feng Z., Xu Z., Tang Y., Li P. and Wu M. (2017). CircRNA: Functions and properties of a novel potential biomarker for cancer. Mol. Cancer 16, 94.

Ratushny V., Gober M.D., Hick R., Ridky T.W. and Seykora J.T. (2012). From keratinocyte to cancer: The pathogenesis and modeling of cutaneous squamous cell carcinoma. J. Clin. Invest. 122, 464-472.

Samarasinghe V., Madan V. and Lear J.T. (2011). Management of high-risk squamous cell carcinoma of the skin. Expert Rev. Anticancer Ther. 11, 763-769.

Sand M., Skrygan M., Georgas D., Sand D., Hahn S.A., Gambichler T., Altmeyer P. and Bechara F.G. (2012). Microarray analysis of microRNA expression in cutaneous squamous cell carcinoma. J. Dermatol. Sci. 68, 119-126.

Sand M., Bechara F.G., Gambichler T., Sand D., Bromba M., Hahn S.A., Stockfleth E. and Hessam S. (2016). Circular RNA expression in cutaneous squamous cell carcinoma. J. Dermatol. Sci. 83, 210-218.

Su H., Tao T., Yang Z., Kang X., Zhang X., Kang D., Wu S. and Li C. (2019). Circular RNA CTFRC acts as the sponge of microRNA-107 to promote bladder carcinoma progression. Mol. Cancer 18, 27.

Wang X., Bu J., Liu X., Wang W., Mai W., Lv B., Zou J., Mo X., Li X., Wang J., Niu B., Fan Y. and Hou B. (2017a). MiR-133b suppresses metastasis by targeting HOXA9 in human colorectal cancer. Oncotarget 8, 63935-63948.

Wang Y., Mo Y., Gong Z., Yang X., Yang M., Zhang S., Xiong F., Xiang B., Zhou M. and Liao Q. (2017b). Circular RNAs in human cancer. Mol. Cancer 16, 25.

Wu J., Qi X., Liu L., Hu X., Liu J., Yang J., Yang J., Lu L., Zhang Z., Ma S., Li H., Yun X., Sun T., Wang Y., Wang Z., Liu Z. and Zhao W. (2019). Emerging epigenetic regulation of circular RNAs in human cancer. Mol. Ther. Nucleic Acids 16, 589-596.

Xia Y.H., Li M., Fu D.D., Xu S.L., Li Z.G., Liu D. and Tian Z.W. (2013). Effects of PTTG down-regulation on proliferation and metastasis of the SCL-1 cutaneous squamous cell carcinoma cell line. Asian Pac. J. Cancer Prev. 14, 6245-6248.

Xiao Y.S., Tong H.Z., Yuan X.H., Xiong C.H., Xu X.Y. and Zeng Y.F. (2020). CircFADS2: A potential prognostic biomarker of colorectal cancer. Exp. Biol. Med. (Maywood) 245, 1233-1241.

You Y., Que K., Zhou Y., Zhang Z., Zhao X., Gong J. and Liu Z. (2018). MicroRNA-766-3p inhibits tumour progression by targeting Wnt3a in hepatocellular carcinoma. Mol. Cells 41, 830-841.

Zhang D.W., Wu H.Y., Zhu C.R. and Wu D.D. (2020). CircRNA hsa_circ_0070934 functions as a competitive endogenous RNA to regulate HOXB7 expression by sponging miR-1236-3p in cutaneous squamous cell carcinoma. Int. J. Oncol. 57, 478-487.

Zhao F., Han Y., Liu Z., Zhao Z., Li Z. and Jia K. (2018). CircFADS2 regulates lung cancer cells proliferation and invasion via acting as a sponge of miR-498. Biosci. Rep. 38.

Zheng X., Huang M., Xing L., Yang R., Wang X., Jiang R., Zhang L. and Chen J. (2020). The circRNA circSEPT9 mediated by E2F1 and EIF4A3 facilitates the carcinogenesis and development of triple-negative breast cancer. Mol. Cancer 19, 73.

Zhong Y., Du Y., Yang X., Mo Y., Fan C., Xiong F., Ren D., Ye X., Li C., Wang Y., Wei F., Guo C., Wu X., Li X., Li Y., Li G., Zeng Z. and Xiong W. (2018). Circular RNAs function as ceRNAs to regulate and control human cancer progression. Mol. Cancer 17, 79.

Zhou L., Wang Y., Zhou M., Zhang Y., Wang P., Li X., Yang J., Wang H. and Ding Z. (2018). HOXA9 inhibits HIF-1α-mediated glycolysis through interacting with CRIP2 to repress cutaneous squamous cell carcinoma development. Nat. Commun. 9, 1480.

Accepted December 16, 2021